Crystal structure, physical properties and superconductivity in A_xFe$_2$Se$_2$ single crystals

X. G. Luo, X. F. Wang, J. J. Ying, Y. J. Yan, Z. Y. Li, M. Zhang, A. F. Wang, P. Cheng, Z. J. Xiang, G. J. Ye, R. H. Liu and X. H. Chen*

Hefei National Laboratory for Physical Science at Microscale and Department of Physics, University of Science and Technology of China, Hefei, Anhui 230026, People's Republic of China

(Dated: February 1, 2011)

We studied the correlation among structure and transport properties and superconductivity in the different A_xFe$_2$Se$_2$ single crystals (A = K, Rb, and Cs). Two sets of (00l) reflections are observed in the X-ray single crystal diffraction patterns, and arise from the intrinsic inhomogeneous distribution of the intercalated alkali atoms. The occurrence of superconductivity is closely related to the c-axis lattice constant, and the A content is crucial to superconductivity. The hump observed in resistivity seems to be irrelevant to superconductivity. There exist many deficiencies within the FeSe layers in A_xFe$_2$Se$_2$, while their T_c does not change so much. In this sense, superconductivity is robust to the Fe and Se vacancies. Very high resistivity in the normal state should arise from such defects in the conducting FeSe layers. A_xFe$_2$Se$_2$ (A = K, Rb, and Cs) single crystals show the same susceptibility behavior in the normal state, and no anomaly is observed in susceptibility at the hump temperature in resistivity. The clear jump in specific heat for Rb$_x$Fe$_2$Se$_2$ and K$_x$Fe$_2$Se$_2$ single crystals shows the good bulk superconductivity in these crystals.

PACS numbers: 74.70.Xa,74.25.F-,74.62.Bf

The newly discovered iron-based superconductors have attracted worldwide attention in the past three years [1–5] because of their high superconducting transition temperature (T_c as high as 55 K) and the fact that superconductivity emerges proximity to the magnetically ordered state. [6, 7], which were considered to be taken as a comparison with the superconducting cuprates for finding out the mechanism of the high-T_c superconductivity. The highest T_c of the FeAs-based pnictides reaches 55 K at ambient pressure, while the anti-PbO type FeSe$_x$, owning the extremely simple structure with the edge-sharing FeSe$_4$ tetrahedra formed FeSe layers stacking along the c-axis, displays a lower T_c of 8 K at ambient pressure [8]. After T_c was enhanced to as high as 37 K by applying high pressure [9], the efforts of introducing structures between the FeSe layers, just like the FeAs-analogues being, successfully induced 30 K superconductivity by intercalating the alkali (K, Rb, Cs) and Tl atoms into between the FeSe layers [10–15]. The intercalated FeSe superconductors show some distinct physical properties from the FeAs-based superconductors, such as, superconductivity with very high normal-state resistivity, a broad hump in resistivity. The Fe content is important in controlling the magnetic and superconducting properties in the iron chalcogenides, additional iron would greatly affect its structural and magnetic properties [16], and superconductivity can be enhanced by the de-intercalation of the interstitial iron [17, 18]. However, vacancies have been found to be able to exist at either A site, or within the conducting FeSe layers in chemical formula A_xFe$_2$Se$_2$, and it is much more complicated than that in the Fe-Se systems. The intercalated alkali atoms could be crucial to the superconductivity. The normal-state resistivity should be influenced by these vacancies seriously. But how these vacancies affect the physical properties still remains unresolved.

In this article, we systematically studied the effect of the starting materials and the heating process on the single crystal growth for A_xFe$_2$Se$_2$ (A = K, Rb, and Cs), and measured the physical properties of these single crystals and determined their crystal structures. It is found that two sets of (00l) reflections exist in all the crystals, and superconductivity is closely related to the c-axis lattice constant, indicating that the A content is crucial to the superconductivity. The hump in resistivity arises from the defects within the conducting FeSe layers and is irrelevant to superconductivity. No anomaly is observed in magnetic susceptibility at the temperature of hump in resistivity. The clear jump in specific heat for superconducting K$_x$Fe$_2$Se$_2$ and Rb$_x$Fe$_2$Se$_2$ single crystals indicates the good bulk superconductivity in these crystals.

Single crystals A_xFe$_2$Se$_2$ (A = K, Rb, and Cs) were grown by Bridgeman method as described elsewhere[12, 13]. The starting materials and the heating process are very important to get superconducting single crystal, and even is slightly changed to dramatically affect its physical properties. The three different batches of Rb$_x$Fe$_2$Se$_2$ and three batches of K$_x$Fe$_2$Se$_2$ single crystals were gotten by the slightly change of the heating temperatures and starting materials. The single crystals were characterized by X-ray single crystal diffraction, magnetic susceptibility, and electrical transport measurements. X-ray single crystal diffraction was performed on a TTRAX3 theta/theta rotating anode X-ray Diffractometer (Japan) with Cu Kα radiation and a fixed graphite monochroma-

*E-mail: chenxh@ustc.edu.cn

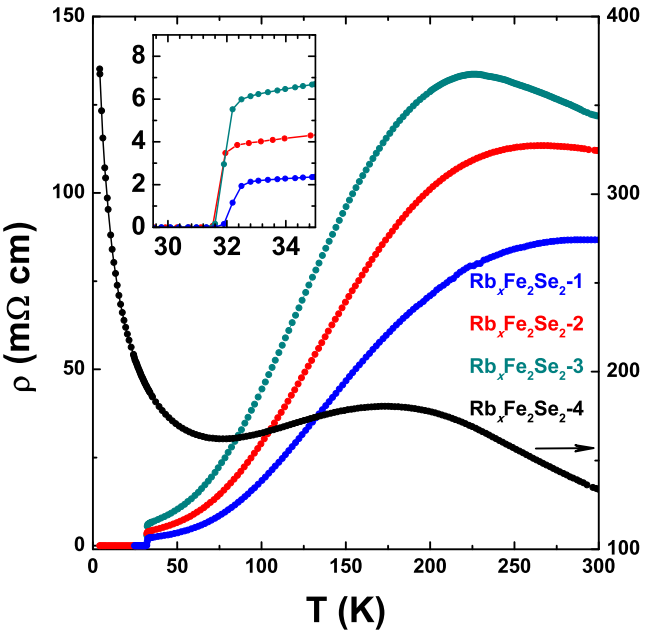

FIG. 1: (Color online) Temperature dependence of resistivity for the three batches of $Rb_xFe_2Se_2$ single crystals: $Rb_xFe_2Se_2$-1 (blue line), $Rb_xFe_2Se_2$-2 (red line), $Rb_xFe_2Se_2$-3 (dark cyan line) and $Rb_xFe_2Se_2$-4 (black line). The inset is zoomed plot of (b) around T_c.

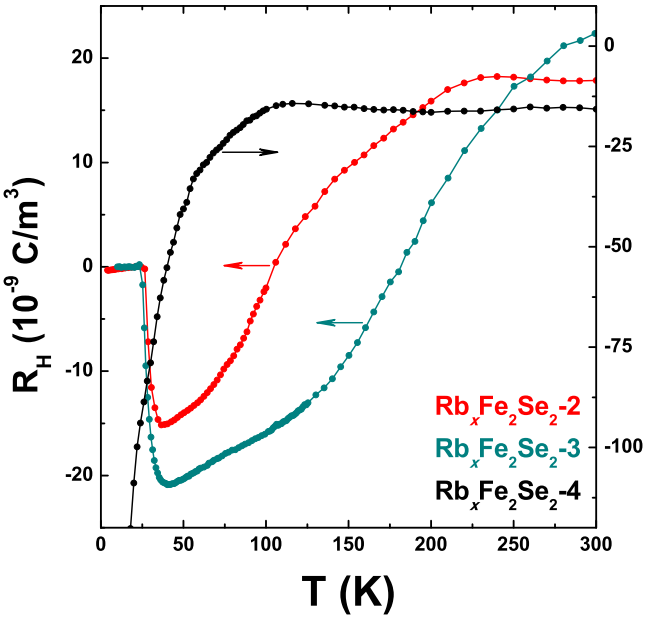

FIG. 2: (Color online) Hall coefficient as a function of temperature for single crystals: $Rb_xFe_2Se_2$-2, $Rb_xFe_2Se_2$-3 and $Rb_xFe_2Se_2$-4.

tor. Magnetic susceptibility measurements were carried out using the *Quantum Design* MPMS-SQUID. The measurement of resistivity and magnetoresistance were done on the *Quantum Design* PPMS-9.

The typical temperature dependence of resistivity is observed for three batches of $Rb_xFe_2Se_2$ single crystals as shown in Fig.1. Among these crystals, $Rb_xFe_2Se_2$-1 was obtained with nominal composition as $Rb_{0.8}Fe_2Se_{1.96}$ by being melt at 1080°C and turning off furnace at 950 °C; $Rb_xFe_2Se_2$-2 and $Rb_xFe_2Se_2$-3 came from the same batch with the nominal composition as $Rb_{0.8}Fe_2Se_2$ by being melt at 1030°C and turning off furnace at 700 °C; $Rb_xFe_2Se_2$-4 was grown with nominal composition as $Rb_{0.8}Fe_2Se_{1.96}$ by being melt at 1030°C and switching off furnace at 700 °C. The resistivity of $Rb_xFe_2Se_2$-1 shows a very small hump around 290 K and then becomes metallic below this temperature with the residual resistivity ratio RRR = R(300 K)/R(35 K) ≈ 37.2. Superconductivity appears below 32.4 K and zero resistance is reached at 31.9 K. The superconducting transition width of $Rb_xFe_2Se_2$-1 is as narrow as 0.5 K although the resistivity at room temperature is as large as 70 mΩ cm at 300 K. The hump temperature of resistivity ($T_{\rm hump}$) shifts to 265 K and 225 K for $Rb_xFe_2Se_2$-2 and $Rb_xFe_2Se_2$-3, respectively. The RRR decreases to 26.1 and 17.3 for the two crystals, respectively. These results indicate that the metallicity of $Rb_xFe_2Se_2$-2 and $Rb_xFe_2Se_2$-3 is weaker compared to $Rb_xFe_2Se_2$-1. However, as we can see from the inset of Fig.1 and Table I, the superconducting transition temperature seems not to vary with the change in the resistivity behavior and their values. The onset and zero resistance temperature for $Rb_xFe_2Se_2$-2 and $Rb_xFe_2Se_2$-3 are 32.0, 32.4 and 31.5, 31.6 K, respectively. Thus one can see that the humps in resistivity seems to be irrelevant to superconductivity. The large magnitude of the normal-state resistivity compared to FeAs-base pnictides [19–21] and FeSe [22] (usually with ρ(300 K) much less than 1 mΩ cm) reflects the existence of many deficiencies within the conducting FeSe layers in these $Rb_xFe_2Se_2$ single crystals. The hump in resistivity should arise from such large amount of defects within the conducting FeSe layers. In this sense, superconductivity is quite robust to the vacancies within the FeSe layers. For $Rb_xFe_2Se_2$-4, although the resistivity still shows a hump at around 170 K, no superconductivity can be observed, and a strong semiconducting/insulator-like behavior is observed below 70 K.

For comparison, we measured the temperature dependence of the Hall coefficient on the exactly same pieces of $Rb_xFe_2Se_2$-2, $Rb_xFe_2Se_2$-3 and $Rb_xFe_2Se_2$-4 as shown in Fig.2. The Hall coefficient of the superconducting crystals $Rb_xFe_2Se_2$-2 and $Rb_xFe_2Se_2$-3 is positive at high temperature, and gradually decreases with decreasing temperature and then becomes negative at low temperature. The sign change of the Hall coefficient is also observed in superconducting $Tl_{0.58}Rb_{0.42}Fe_{1.72}Se_2$ samples previously [23]. Actually from ARPES results in $A_xFe_2Se_2$ (A = K and Cs) [24, 25], the $A_xFe_2Se_2$ are electron over-doped and only electron pockets can be observed. However, hole pockets could exist in the superconducting samples due to sign change of Hall coefficient based on the Hall effect measurements, suggesting a pos-

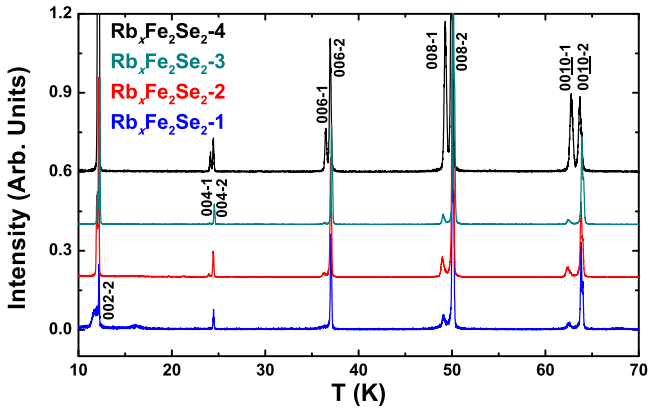

FIG. 3: (Color online) The X-ray single crystal diffraction patterns for the different batches $Rb_xFe_2Se_2$ single crystals.

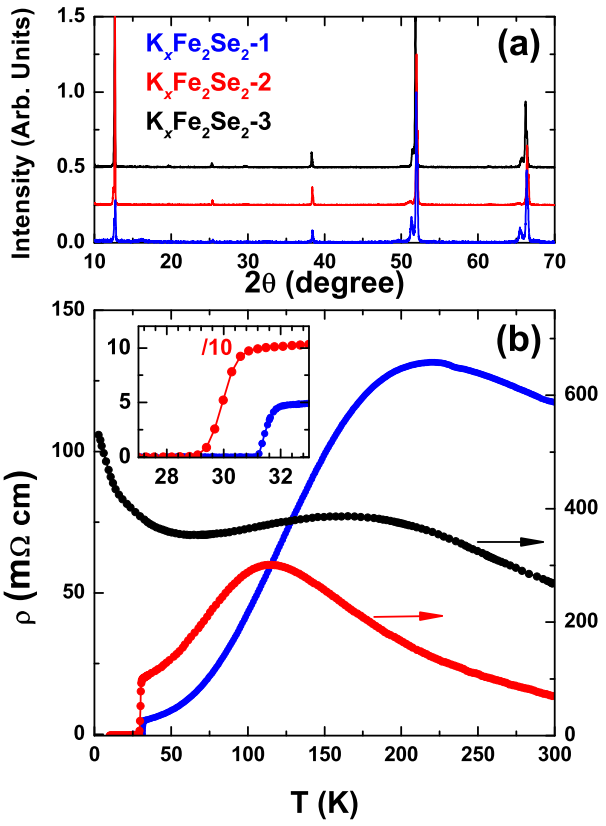

FIG. 4: (Color online) (a): The X-ray single crystal diffraction patterns for the different batches $K_xFe_2Se_2$ single crystals: $K_xFe_2Se_2$-1 (blue line), $K_xFe_2Se_2$-2 (red line) and $K_xFe_2Se_2$-3 (black line); (b): The temperature dependence of the resistivity of these three different $K_xFe_2Se_2$ single crystals. The inset is zoomed plot of (b) around T_c.

sibly multi-band nature of the superconductivity. For the sample without superconductivity, the Hall coefficient is negative in the whole temperature range. It indicates that dominant carrier is electron for non-superconducting crystal. It seems that the hole pocket might be quite important for the superconductivity. Therefore, it needs to be further investigated. What's more, no anomaly in the Hall coefficient is observed at $T_{\rm hump}$. It suggests that the humps in resistivity for $A_xFe_2Se_2$ crystals are not related to a structural or magnetic transition, being contrasting to the facts that the anomaly of resistivity in underdoped FeAs-based superconductor is always relevant to a structural/magnetic transition.

As shown in Fig. 1, one can observe almost the same T_c for the single crystals with the different $T_{\rm hump}$. The X-ray single crystal diffraction was carried out for the same four pieces $Rb_xFe_2Se_2$ single crystals shown in Fig. 1 to find out the relationship of superconductivity and structure. The X-ray diffraction (XRD) patterns are shown in Fig. 3. Surprisingly, two sets of $(00l)$ reflections are observed in all the four samples. The two c-axis lattice parameters $c1$ and $c2$ are obtained (listed in Table I). The c-axis lattice parameters $c1$ and $c2$ correspond to the two sets of reflections with weak and strong intensities, respectively. These two distinct sets of reflections could arise from the inhomogeneous distribution of the intercalated Rb atoms. Considering the fact that the superconducting crystals show nearly fully shielding fraction, the reflections with $c2$ should be responsible for the superconductivity. From the superconducting to non-superconducting crystal, $c1$ is reduced by 0.55% while $c2$ is enhanced by more than 0.14%. It is found that the insulator-like behavior is enhanced with losing superconductivity. It indicates that superconductivity may exist within a limited range of the c-axis lattice parameter. In other word, the Rb content is crucial to the occurrence of superconductivity because the c-axis lattice parameter strongly depends on the Rb content.

We then carefully measured resistivity and the XRD patterns for three pieces of $K_xFe_2Se_2$ crystals, as shown in Fig. 4 . It shows that the $K_xFe_2Se_2$ crystals exhibit the obviously different resistivity behavior. $K_xFe_2Se_2$-1 was grown using $K_{0.8}(FeSe)_2$ as starting materials and being melt at 1030 °C for 3 hours. $K_xFe_2Se_2$-2 and $K_xFe_2Se_2$-3 were grown by using $K_{0.8}(FeSe)_2$ as starting materials and being melt at 1030 °C for 2 hours and 950 °C for 20 hours, respectively. In Fig.4a, two sets of $(00l)$ reflections can be observed, and this behavior is the same with those in the $Rb_xFe_2Se_2$ samples, suggesting that the inhomogeneous distribution of the intercalated alkali atoms in the crystals is common feature. For the non-superconducting sample, the c-axis lattice constant $c1$ is smaller by more than 0.64%, while $c2$ is larger by 0.15% than those in the superconducting samples. These results are consistent with the results observed in the $Rb_xFe_2Se_2$ samples, indicating that the content of alkali atom plays a crucial role for the occurrence of superconductivity. $K_xFe_2Se_2$-1 shows a broad resistivity hump at about 220 K and superconductivity at 31.7 K. For the $K_xFe_2Se_2$-2, $T_{\rm hump}$ shifts to 120 K and superconductivity shows up at 30.3 K. Although the superconductivity disappears in $K_xFe_2Se_2$-3, the $T_{\rm hump}$ for $K_xFe_2Se_2$-3 is higher than that for the superconducting $K_xFe_2Se_2$-2, strongly demonstrating that

TABLE I: The c-axis lattice parameters $c1$ and $c2$ corresponding to the two sets of reflections with weak and strong intensities, respectively. T_c^{zero}, T_c^{onset}, the hump temperature in resistivity (T_{hump}) and residual resistivity ratio (RRR = R(300 K) / R(35 K)) for all the crystals $A_xFe_2Se_2$ (A=K, Rb, Cs).

sample name	$c1$ (Å)	$c2$ (Å)	T_c^{zero} (K)	T_c^{onset} (K)	T_{hump} (K)	RRR
$Rb_xFe_2Se_2$-1	14.873	14.569	31.9	32.4	290	37.2
$Rb_xFe_2Se_2$-2	14.873	14.582	31.5	32.0	265	26.1
$Rb_xFe_2Se_2$-3	14.874	14.574	31.6	32.4	225	17.3
$Rb_xFe_2Se_2$-4	14.792	14.604			170	
$K_xFe_2Se_2$-1	14.292	14.086	31.2	31.7	220	21.2
$K_xFe_2Se_2$-2	14.282	14.062	29.2	30.8	120	0.65
$K_xFe_2Se_2$-3	14.201	14.107			160	
$Cs_xFe_2Se_2$	15.556	15.285	28.3	30.3	no hump <300 K	16.3

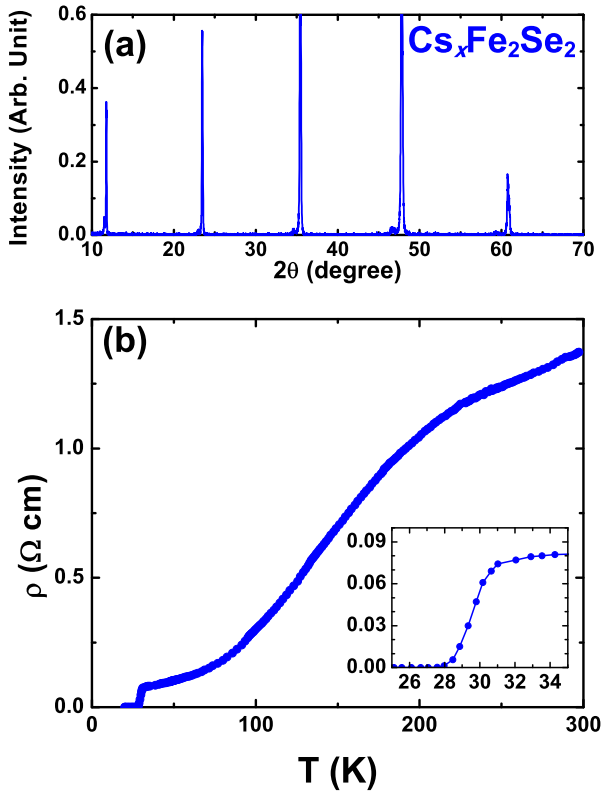

FIG. 5: (Color online) (a): The X-ray single crystal diffraction pattern for the $Cs_xFe_2Se_2$ single crystal; (b): The temperature dependence of the resistivity of the $Cs_xFe_2Se_2$ single crystal. The inset is zoomed plot of (b) around T_c.

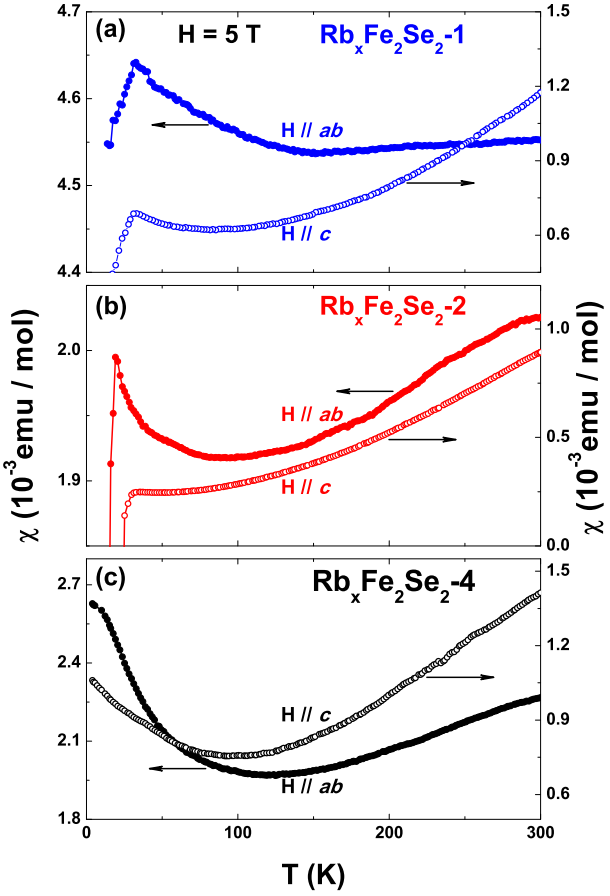

FIG. 6: (Color online) The temperature dependence of the susceptibility with the magnetic field of 5T applied parallel and perpendicular to the c-axis for (a): $Rb_xFe_2Se_2$-1; (b): $Rb_xFe_2Se_2$-2; (c): $Rb_xFe_2Se_2$-4.

the superconductivity is not correlated to the hump in resistivity. The position of the hump in resistivity reflects the vacancy level within the conducting FeSe layers. It suggests that the vacancies within the FeSe layers have much weaker correlation to superconductivity than the content of intercalated alkali atoms does.

Figure 5 shows the X-ray single crystal diffraction pattern and the temperature dependence of resistivity for $Cs_xFe_2Se_2$ single crystal. Totally metallic resistivity can be observed below 300 K. Superconductivity was observed with T_c^{onset} = 30.3 K and T_c^{zero} = 28.3 K. In the XRD patterns of Fig.5a, very small reflections corresponding to $c1$ can still be found except for the main reflections with $c2$. It suggests the inhomogeneous distribution of alkali atoms is common for all the $A_xFe_2Se_2$ single crystals. It is worthy to note that the superconductivity always shows up around 30 K for the crystals $A_xFe_2Se_2$

with changing the intercalated alkali atom A from K, Rb to Cs. The T_c seems not to depend on the ionic radii of the intercalated alkali atoms although the superconductivity strongly depends on the A content. As shown in Fig.1 and Fig.4b, the hump in resistivity changes pronouncedly for the same alkali atom case, while the T_c is nearly the same (about 30 K). Very large normal-state resistivity is observed in all the above $A_xFe_2Se_2$ single crystals, suggesting that large amount of deficiencies within the conducting FeSe layers for all of these crystals. Based on these observations, T_c seems to be robust to the vacancies within the FeSe layers.

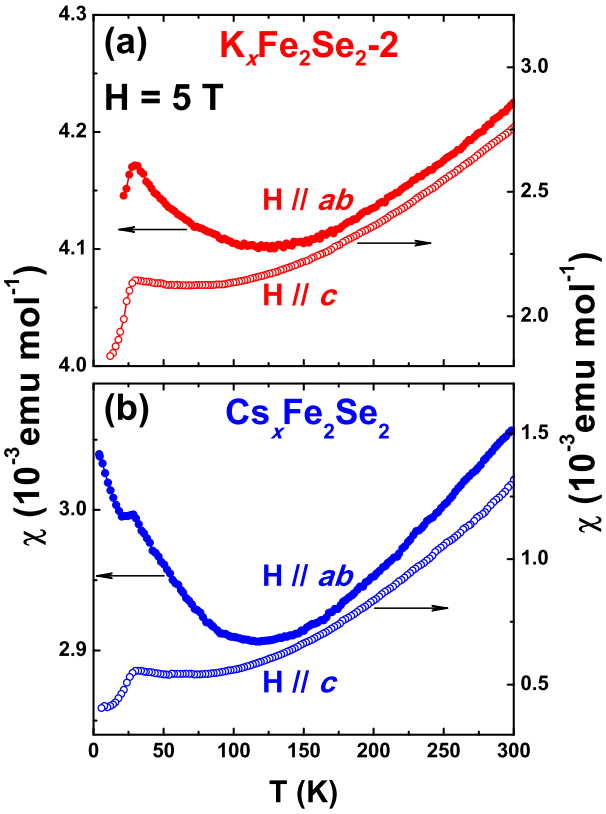

FIG. 7: (Color online) The temperature dependence of the susceptibility with the magnetic field of 5 T applied parallel and perpendicular to the c-axis for (a): $K_xFe_2Se_2$-2; and (b): $Cs_xFe_2Se_2$.

Magnetic susceptibility was measured on the $A_xFe_2Se_2$ single crystals to investigate the correlation between the normal-state resistivity and magnetism. Figure 6 shows the anisotropic magnetic susceptibility with the magnetic field of 5 T applied within the ab-plane and along the c-axis for $Rb_xFe_2Se_2$-1, $Rb_xFe_2Se_2$-2, $Rb_xFe_2Se_2$-4, respectively. Although the samples show very different resistivity behavior, such as the different T_{hump}s, the magnitude of resistivity and T_c, the normal-state susceptibility shows the quite similar behavior to each other. As the field is applied within the ab-plane, the magnitude of susceptibility varies within 20% in the normal state and the susceptibility itself shows a broad minimum. No anomaly can be found at T_{hump}, suggesting that hump in resistivity cannot be ascribed to a magnetic transition. Fig.7 shows the susceptibility with the magnetic field of 5 T applied parallel and perpendicular to the c-axis for $K_xFe_2Se_2$-2 and $Cs_xFe_2Se_2$, respectively. The similar behavior with those of $Rb_xFe_2Se_2$ crystals shown in Fig.6 is observed. These results indicate that although the electronic properties change dramatically from system to system and from crystal to crystal, the magnetic property does not change a lot.

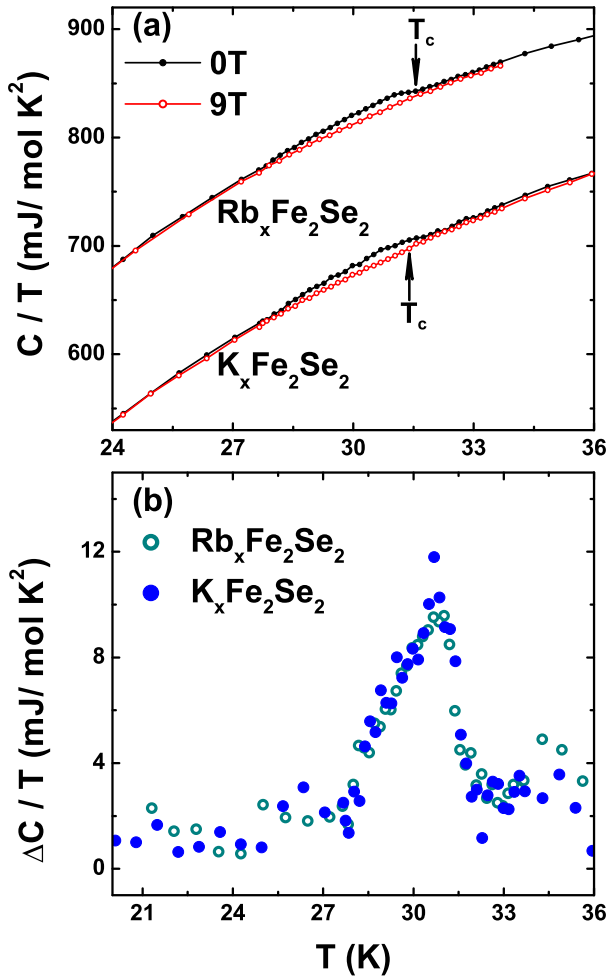

FIG. 8: (Color online) (a): The heat capacity as a function of temperature for $Rb_xFe_2Se_2$-2 and $K_xFe_2Se_2$-1 at the magnetic field of 0T and 9T applied along c-axis. (b): The heat capacity difference between 0T and 9T for $Rb_xFe_2Se_2$-2 and $K_xFe_2Se_2$-1. A clear heat peak was observed, indicating the good bulk superconductivity.

Fig.8a shows the temperature dependence of the specific heat (C/T) around T_c at the magnetic field of 0 T and 9 T for $Rb_xFe_2Se_2$-2 and $K_xFe_2Se_2$-1, respectively. At 0 T, one can see the clear specific heat anomaly at T_c. Although 9 T is far lower than the upper critical field, which is estimated higher than 100 T,[12, 13] the anomaly in specific heat is completely suppressed. The specific heat jump (C(0T)-C(9T))/T against T is plot-

ted in Fig.8b for the two crystals. The heat capacity jumps for $Rb_xFe_2Se_2$-2 and $K_xFe_2Se_2$-1 crystals shows almost the same behavior. The clear heat capacity jump in the superconducting samples definitely indicates the good bulk superconductivity in these crystals.

The X-ray single crystal diffraction patterns reveals two sets of $(00l)$ reflections existing in all the crystals of $A_xFe_2Se_2$. Such two sets of reflections strongly depend on the starting composition and heating process. Although the superconducting phase is dominant, the trace of second phase is still observed as shown in Fig.5a. These results indicate the existence of inhomogeneous distribution of the A atoms in all the crystals. It is found that superconductivity is closely related to the c-axis lattice constant, indicating that the A content is crucial to the superconductivity because the c-axis lattice parameter strongly depends on the A content. The A content in single crystals is quite sensitive to the nominal composition and condition of crystal growth. Therefore, it is not easy to grow the single crystal with superconductivity. The very large normal-state resistivity relative to other iron pnictide superconductors suggests the large amount of deficiencies within the conducting FeSe layers for all the $A_xFe_2Se_2$ single crystals. The hump in resistivity should arise from such defects, and seems to be irrelevant to superconductivity. Despite of the existence of many deficiencies within the conducting FeSe layers in $A_xFe_2Se_2$, T_c does not change a lot with varying A from K to Rb and Cs. Therefore, superconductivity seems robust to the such vacancies. No anomaly is observed in magnetic susceptibility at the hump temperature in resistivity. It suggests that the humps in resistivity in $A_xFe_2Se_2$ are not related to a structural or magnetic transition, being contrasting to the facts that the anomaly of resistivity in the underdoped FeAs-based superconductor is always relevant to a structural/magnetic transition.

In conclusion, we systematically studied the structure by the X-ray single crystal diffraction and measured the transport properties in the $A_xFe_2Se_2$ single crystals. All the samples show two sets of $(00l)$ reflections in X-ray single crystal diffraction patterns, indicating the intrinsically inhomogeneous distribution of the intercalated A atoms. The occurrence of Superconductivity is closely related to the c-axis lattice parameter, indicating that the A content is crucial to the superconductivity in $A_xFe_2Se_2$. The very large magnitude of the normal-state resistivity reflects the large amount of deficiencies within the conducting FeSe layers. The hump in resistivity should originate from these defects and is found to be irrelevant to the superconductivity. In this sense, superconductivity is robust to the vacancies within the FeSe layers. No anomaly in susceptibility is observed to be associated with the hump in resistivity. The clear jump in specific heat for $Rb_xFe_2Se_2$ and $K_xFe_2Se_2$ superconducting single crystals indicates the good bulk superconductivity in these crystals.

ACKNOWLEDGEMENT This work is supported by the Natural Science Foundation of China and by the Ministry of Science and Technology of China, and by Chinese Academy of Sciences.

[1] Yoichi Kamihara, Takumi Watanabe, Masahiro Hirano and Hideo Hosono, J. Am. Chem. Soc. **130**, 3296 (2008).
[2] X. H. Chen, T. Wu, G. Wu, R. H. Liu, H. Chen and D. F. Fang, Nature **453**, 761(2008).
[3] Z. A. Ren, W. Lu, J. Yang, W. Yi, X. L. Shen, Z. C. Li, G. C. Che, X. L. Dong, L. L. Sun, F. Zhou and Z. X. Zhao, Chin. Phys. Lett. **25** , 2215(2008).
[4] M. Rotter, M. Tegel, D. Johrendt, Phys. Rev. Lett. **101**, 107006(2008).
[5] R. H. Liu, G.Wu, T. Wu, D. F. Fang, H. Chen, S. Y. Li, K. Liu, Y. L. Xie, X. F.Wang, R. L. Yang, L. Ding, C. He, D. L. Feng and X. H. Chen, Phys. Rev. Lett. **101**, 087001 (2008).
[6] H. Chen, Y. Ren, Y. Qiu, Wei Bao, R. H. Liu, G. Wu, T. Wu, Y. L. Xie, X. F. Wang, Q. Huang and X. H. Chen, Europhys. Lett. **85**, 17006(2009).
[7] Clarina de la Cruz, Q. Huang, J. W. Lynn, Jiying Li, W. Ratcliff II, J. L. Zarestky, H. A. Mook, G. F. Chen, J. L. Luo, N. L. Wang and Pengcheng Dai, Nature **453** 899 (2008).
[8] F. C. Hsu, J. Y. Luo, K. W. The, T. K. Chen, T. W. Huang, P. M. Wu, Y. C. Lee, Y. L. Huang, Y. Y. Chu, D. C. Yan and M. K. Wu, Proc. Nat. Acad. Sci. **105**, 14262 (2008).
[9] S. Medvedev, T. M. McQueen, I. Trojan, T. Palasyuk, M. I. Eremets, R. J. Cava, S. Naghavi, F. Casper, V. Ksenofontov, G. Wortmann and C. Felser, Nature Mater. **8** 630(2009)
[10] J. Guo, S. Jin, G. Wang, S. Wang, K. Zhu, T. Zhou, M. He and X. Chen, Phys. Rev. B **82**, 180520 (2010).
[11] Yoshikazu Mizuguchi, Hiroyuki Takeya, Yasuna Kawasaki, Toshinori Ozaki, Shunsuke Tsuda, Takahide Yamaguchi and Yoshihiko Takano, arXiv:1012.4950 (unpublished).
[12] A. F. Wang, J. J. Ying, Y. J. Yan, R. H. Liu, X. G. Luo, Z. Y. Li, X. F. Wang, M. Zhang, G. J. Ye, P. Cheng, Z. J. Xiang, X. H. Chen, arXiv:1012.5525 (unpublished).
[13] J. J. Ying, X. F. Wang, X. G. Luo, A. F. Wang, M. Zhang, Y. J. Yan, Z. J. Xiang, R. H. Liu, P. Cheng, G. J. Ye, X. H. Chen , arXiv:1012.5552 (unpublished).
[14] A. Krzton-Maziopa, Z. Shermadini, E. Pomjakushina, V. Pomjakushin, M. Bendele, A. Amato, R. Khasanov, H. Luetkens and K. Conder, arXiv:1012.3637 (unpublished).
[15] Minghu Fang, Hangdong Wang, Chiheng Dong, Zujuan Li, Chunmu Feng, Jian Chen, H.Q. Yuan, arXiv:1012.5236 (unpublished).
[16] Wei Bao, Y. Qiu, Q. Huang, M. A. Green, P. Zajdel, M. R. Fitzsimmons, M. Zhernenkov, S. Chang, Minghu Fang, B. Qian, E. K. Vehstedt, Jinhu Yang, H. M. Pham, L. Spinu, and Z. Q. Mao, Phys. Rev. Lett. **102**, 247001

(2009).
[17] M. Bendele, P. Babkevich, S. Katrych, S. N. Gvasaliya, E. Pomjakushina, K. Conder, B. Roessli, A. T. Boothroyd, R. Khasanov, and H. Keller, Phys. Rev. B **82**, 212504 (2010).
[18] E. E. Rodriguez, C. Stock, P-Y Hsieh, N. Butch, J. Paglione, M. A. Green, arXiv:1012.0590 (unpublished).
[19] X. F. Wang, T. Wu, G. Wu, R. H. Liu, H. Chen, Y. L. Xie, and X. H. Chen, New Journal of Physics **11**, 045003 (2009).
[20] H. Q. Luo, Z. S. Wang, H. Yang, P. Cheng, X. Y. Zhu, and H. H. Wen, Supercond. Sci. Technol. **21**, 125014 (2008).
[21] P. Cheng, H. Yang, Y. Jia, L. Fang, X. Y. Zhu, G. Mu, and H. H. Wen, Phys. Rev. B **78**, 134508 (2008).
[22] D. Braithwaite, B. Salce1, G. Lapertot, F. Bourdarot, C. Marin, D. Aoki, and M. Hanfland, J. Phys.: Condens. Matter **21**, 232202 (2009).
[23] H. D. Wang, C. H. Dong, Z. J. Li, S. S. Zhu, Q. H. Mao, C. M. Feng, H. Q. Yuan, and M. H. Fang, arXiv:1101.0462 (unpublished).
[24] Y. Zhang, L. X. Yang, M. Xu, Z. R. Ye, F. Chen, C. He, J. Jiang, B P. Xie, J. J. Ying, X. F. Wang, X. H. Chen, J. P. Hu, and D. L. Feng, arXiv:1012.5980 (unpublished).
[25] T. Qian, X.-P. Wang, W.-C. Jin, P. Zhang, P. Richard, G. Xu, X.Dai, Z.Fang, J.-G Guo, X.-L. Chen, and H. Ding, arXiv:1012.6017 (unpublished).